MIJST
MIST International Journal of Science and Technology

Seismic Performance Evaluation of a Fire-Damaged Reinforced Concrete High Rise Building by Non-linear Time History Analysis

Md Abdul Momin* and Khondaker Sakil Ahmed

Department of Civil Engineering, Military Engineering of Science and Technology, Dhaka, Bangladesh

***Corresponding Email:** *momin.ce09@gmail.com*

ARTICLE INFO

Article History:

Received: 02nd July 2025
Revised: 12th November 2025
Accepted: 12th January 2026
Published: 30th June 2026

Keywords:

Damage Assessment
ACI562
Residual Strength
Heat Transfer Analysis
Performance-Based Analysis

ABSTRACT

Concrete is widely used worldwide for the construction of buildings and infrastructure that remain stable under fire. It shows some damage and deformations that require maintenance. Although rehabilitation and restoration procedures for fire-damaged buildings are usually time-consuming and costly, the post-fire resilience of the structure is very important for understanding its capacity and condition. In the seismic zone, the buildings must satisfy the seismic demand after the potential repair and retrofitting of the fire-damaged building. A simple, verified simulation procedure for post-fire seismic analysis is necessary to advance understanding of the seismic performance of RC structures after fire. However, individual computer programs that can perform well in both thermal and seismic analysis may help structural engineers make decisions. This study presents an in-depth seismic performance evaluation of a fire-damaged high-rise reinforced concrete (RC) building in Dhaka, Bangladesh. The building, which suffered severe fire damage on the 7th to 9th floors, underwent rigorous structural investigation and testing, including core extraction and rebar tensile testing. According to ACI 562, the residual strengths of concrete and reinforcement were calculated. A comprehensive finite element model was developed in ETABS to simulate the structure's static and dynamic behavior. Nonlinear Time History Analysis (NLTHA) was performed using nine ground motion records scaled to Bangladesh National Building Code (BNBC 2020) spectra. The comparative results are presented in terms of storey drift and displacement, stiffness, and demand /capacity ratios of column and shear wall. In most cases, it meets the allowable limits for different performance criteria. The proposed assessment procedure can capture the actual conditions of a fire-damaged building at different performance levels, helping stakeholders make further strategic decisions about the damaged structure.

This work is licensed under a *Creative Commons Attribution-Non-commercial 4.0 International License.*

1. INTRODUCTION

The fire initially discovered by early hominids has evolved into a crucial part of contemporary life. It can occasionally cause unforeseen events in any structure, leading to catastrophic structural damage and serious loss of life and property. Building construction cannot be undertaken without considering fire impacts due to several challenges (Poliakova & Grigoryan, 2018; Wang et al., 2011), despite the unfavorable consequences of fire on structural materials. Some safety measures should be considered when designing in order to overcome these difficulties. EN 1991-1-2, ISO 834 (1999), the International Building Code (IBC) (ICC, 2012), and ASTM E119 design regulations can be used for structural fire design. Fire resistance is a concept applicable to building structural elements rather than to a material, but even a material's properties can affect the performance of an element (Khoury, 2000). By running common fire tests according to standard procedures, someone might determine the fire resistance of reinforced concrete structural elements with appropriate precautions. The codes ISO 834 (ISO, 1999), EN 1991-

1-2 (CEN, 2002), EN 1992-1-2 (CEN, 2004), International Building Code (IBC) (ICC, 2012), and ASTM E119 could be used to determine measures to address a potential fire (ASTM, 2016). When structural resistance is assessed, failure criteria are usually defined in terms of load-bearing capacity, level, and rate of deformation (Bailey, 2004). The time span of acceptable behavior is then used to express the element's fire resistance, and this time span is either reported in terms of critical temperatures at specific areas or in terms of the element's ability to withstand load during testing. During fire, thermal expansion and thermal bowing of the structural elements, rather than material degradation or gravity loading, governed the response to fire(Jowsey et al., 2005). The load-carrying capacity of an element can be calculated based on the temperature distribution within the element, disregarding transient time-temperature states, using certain other limit-state approaches to fire resistance (Anderberg & Thelandersson, 1976; Lie et al., 1972). Parametric fire curve development can help to estimate the maximum gas temperature of the compartment (Benýšek et al., 2020; EN, 1991; Ma & Mäkeläinen, 2000; Zehfuss & Hosser, 2007). Some finite element software can be used to determine the time temperature (Block et al., 2010; Keerthan & Mahendran, 2013).

The consensus is that steel structures are less fire-resistant than reinforced concrete structures. In contrast, concrete structural members [mostly fabricated from normal strength concrete NSC)] exhibit good performance under fire situations. The most likely justification for this viewpoint is the presumption that concrete maintains its cross-sectional integrity in the presence of fire (Huang, 2010). Conversely, when exposed to high temperatures, concrete's chemical and physical characteristics change. A decrease in the strength of the concrete and a reduction in the cross-section area of the reinforced concrete elements may be caused, in brief, by changing the water content, chemical structure, pore distribution and density, microstructure, and explosive sloughing-off or spalling occurrences (Ali et al., 2001; Bailey, 2002; Chan et al., 2000; Lin et al., 1996).

It is possible to assess the temperature-induced loss of strength in steel rebar and concrete by knowing the temperatures in the rebar and concrete layers. Typically, when steel is cooled, it regains the majority of its strength and stiffness. However, the residual strength of rebar steel decreases with increasing maximum temperature, especially when it exceeds 500 ^{o}C. According to the temperature-residual strength test results published by Neves et al., the proposed design approach assumes that the loss of strength in reinforcing steel will be proportional to the temperature (Neves et al., 1996). Due to the loss of concrete confinement, the steel rebar between two adjacent stirrups behaves as distinct compression bars and buckles when the level of spalling is such that the cover concrete completely spalls off the steel rebar. It is necessary to use a buckling strength reduction coefficient to consider this local buckling. According to a recent study (Jiang et al., 2007)The diameter and initial strength of steel bars, the spacing between stirrups, and the first bending displacement of steel bars all significantly affect the strength reduction coefficient. The strain-hardening effect in rebar is another factor that may influence residual strength. A strain-hardening factor can be used to evaluate the residual strength of rebar when accurate information on its strength properties is available. However, relatively little information is available regarding the effects of strain hardening on reinforcing steel, particularly after cooling.

Several publications guide the procedure for evaluating fire-damaged concrete structures (Felicetti, 2013, 2014; Mo et al., 2004; Momin et al., 2024). The Concrete Society Technical Report 15 is the most comprehensive and practical technical report, comprising three main parts: damage assessment, design, and repair methods (Tovey, 1986). Research at the Technical University of Braunschweig has focused heavily on fire-affected concrete materials and structures (Kordina & Krampf, 1984). Similarly, the Portland Cement Association in the United States has conducted several studies on concrete structures and fire.

The inelastic behavior of reinforced concrete components and joints under seismic loads has been the subject of extensive experimental research during the past three decades. Previous research on columns and beams has demonstrated that several structural factors, including concrete strength, longitudinal steel ratio, shear span ratio, stirrup ratio, infill wall ratio, and axial stress level, affect the structural deformation and energy-absorbing characteristics. These factors may be seen as strength loss, stiffness loss, and pinching behavior in the load-deformation relation (Duan & Hueste, 2012; Lu, 2002; Mallick et al., 2026; Sadjadi et al., 2007; Seo et al., 2015). The residual capacity of a structural member depends on the aforesaid factors. All these complexities can be particularly evident when the structures are subjected to significant dynamic loads, such as strong seismic ground motions (Anam et al., 2003). Based on knowledge of the hysteretic behavior of components, numerous studies have been conducted to get a realistic simulation of the inelastic dynamic response of reinforced concrete frames (Galal & Ghobarah, 2003; Roufaiel & Meyer, 1987; Sengupta & Li, 2014; Xun-Liu et al., 2007).

In this research, a detailed performance analysis of a 23-storied fire-affected reinforced concrete structure has been done. The results of the linear force-based analysis have been compared for pre- and post-fire conditions, in accordance with the Bangladesh National Building Code 2020 (BNBC 2020). Fire stress analysis helps predict the residual strength of materials, such as concrete and rebar. Furthermore, a nonlinear time-history analysis was conducted, accounting for reduced material strength. Finally, the comparative seismic performance criteria (displacement, drift, base shear, fiber stress-strain, and hinge rotation) have been assessed accordingly.

2. METHODOLOGY

The purpose of this research is to focus on the seismic vulnerability assessment of a fire-damaged reinforced concrete structure (as shown in Figure 1) that integrates visual assessments, materials testing, and advanced finite element simulations. The methodology consisted of the following main phases: site visit; data collection and material testing; fire simulation and thermal degradation modeling; structural modeling and analysis using ETABS; and seismic demand evaluation through nonlinear time-history analysis (NLTHA).

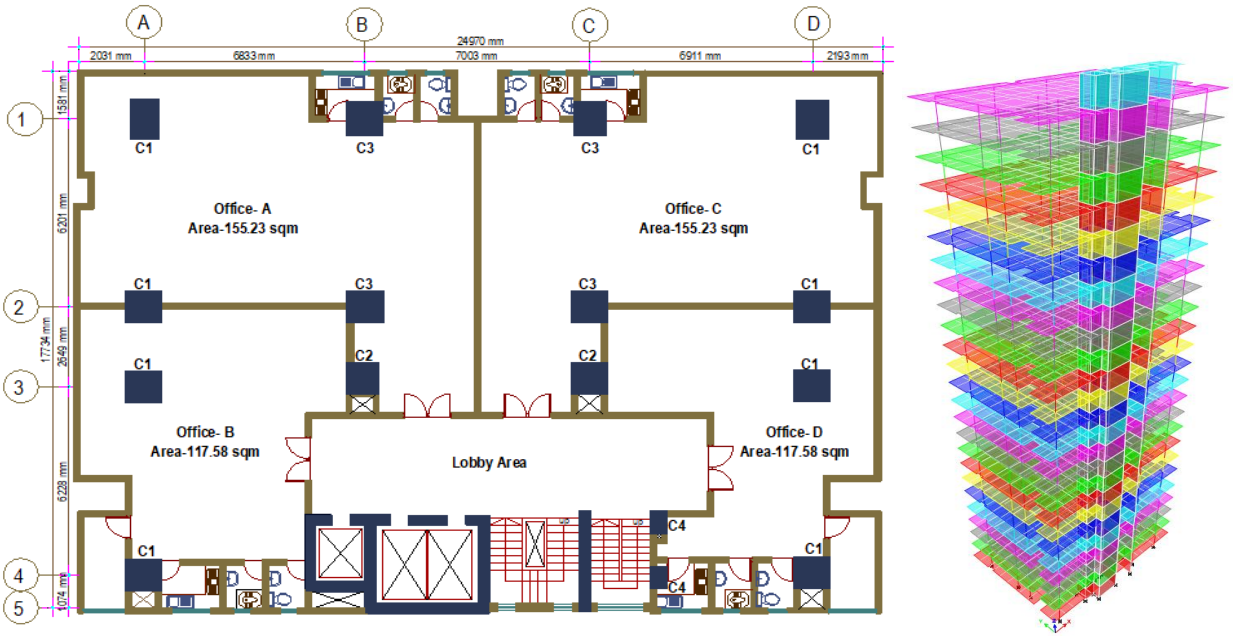

Figure 1: Typical floor plan and 3D view of the building

2.1 Material Testing and Strength Evaluation

Visual inspections were conducted to identify concrete spalling, cracking, discoloration, and deformation following the fire. Subsequently, the structural members were examined to determine the exact location of the core sampling. Concrete core samples were extracted from fire- exposed and unaffected zones with proper precautions. In accordance with ASTM C42/C42M, the compressive strength of core samples was tested. Moreover, the post-fire yield and ultimate strength of rebar samples were assessed by collecting and testing tensile specimens.

The residual strength of concrete and rebar is calculated according to ACI 562, which provides reduction factors for fire exposure duration, temperature, thermal profiles through cross sections, etc. The guidelines for temperature-dependent material degradation curves in Eurocode (EN 1992-1-2) were used to calculate post-fire strength reduction (CEN 2004).

2.2 Fire Temperature Simulation and Heat Transfer Modelling

In fire engineering design of buildings and structural components, most frequently a classification system and related standard tests, such as ISO 834, EN 1363-1, or ASTM E-119, with specified time-temperature fire exposures, are used. A parametric fire curve was developed to assess thermal effects in accordance with EN 1991-1-2 Annex A, which accounts for fire load density, ventilation, and compartment dimensions. The duration of the fire and peak temperatures at different locations within the structure are assessed through simulation. Anderberg and Thelandersson (1976) outlined some assumptions regarding heat transfer mechanisms. The thermal heat transfer gradient (Figure 2) for columns and beams is determined using 2D heat transfer analysis in FIN EC software.

The conduction method was used to transfer heat through the concrete and rebar sections, whereas radiation/ convection mechanisms were used at the boundary layers. In solids, heat conduction was described by Fourier's law. The gradient temperature of the rebar-concrete section was then calculated at each instance for later thermal stress analysis. The maximum heated temperature in the outer layer of concrete and at the corner rebar was determined to be more than 900 °C and 700 °C, respectively. Empirical models of Kodur et al. were used to distribute temperature into rebar and concrete temperature-time histories, which were then used to calculate strength degradation (Kodur et al., 2003).

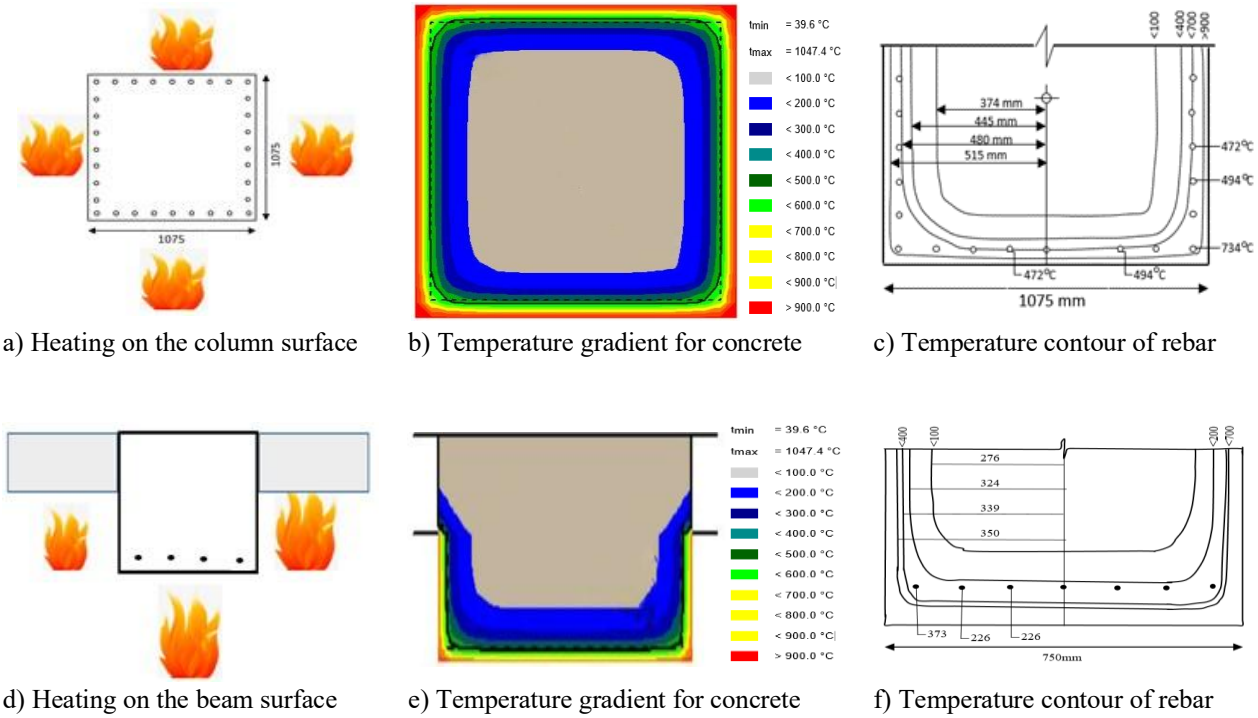

a) Heating on the column surface b) Temperature gradient for concrete c) Temperature contour of rebar

d) Heating on the beam surface e) Temperature gradient for concrete f) Temperature contour of rebar

Figure 2: Temperature distribution in column and beam sections.

2.3 Structural Modeling for Finite Element Analysis

A 3D finite element analysis of a 22-storey building with two (02) existing basement buildings is modelled using the commercial design software ETABS from CSI Inc. The basic dimensions are kept at 24.97 m in the x-direction and 17.73 m in the y-direction. The building is 67.85m high and has a typical story height of 3.05m. The basement and ground to third-floor height are 2.8m and 3.3m, respectively. Both geometric and material non-linearity are considered in the analysis procedure.

2.3.1 Section and material properties

The sizes of the columns C1, C2, C3, and C4 are 975 x 1225 mm, 1075 x 1075 mm, 1200 x 1200 mm, and 375 x 1050 mm, respectively, at the ground floor as shown in Figure 3. Column size has changed at the ground, third, fifth, seventh, tenth, and seventeenth-floor levels. The cross-sectional dimension of the beam is 750 × 400 mm. The thickness of all the shear walls is 300 mm. The overall slab thickness is 187.5 mm with a column capital of 62.5 mm.

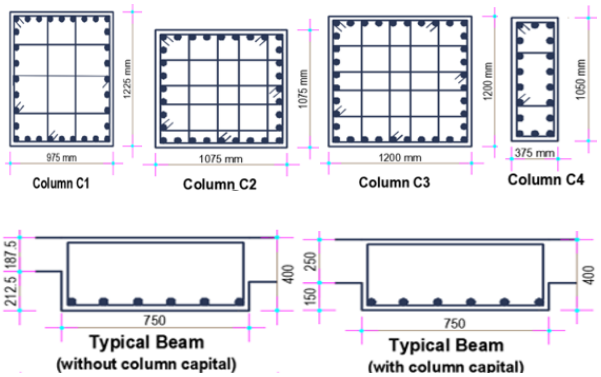

Figure 3: Cross-section of columns and beam with rebar arrangements

The densities of concrete and brick walls are 24 kN/m3 and 20 kN/m3, respectively. The material properties have been considered as per Table 1.

Table 1: Properties of fire-affected and unaffected concrete. (Source: ASCE 41-17)

Material Property		Value	
		Fire unaffected	Fire affected
Concrete compressive strength, f'c (MPa)	Column	36.6	24.5
	Beam & Slab	30.3	23.5
Modulus of Elasticity, E(MPa)		$4700*\sqrt{f'c}$	
Rebar Yield Strength, fy(MPa)		420	392
Exp.Tensile Strength, fu (MPa)		491*	458.6*
Modulus of Elasticity, E(MPa)		21000	

*Expected tensile strength factor for nonlinearity- 1.3(concrete) & 1.17(reinforcement);

The load patterns, seismic parameters, and combinations from the Bangladesh National Building Code 2020, as presented in Table 2, were used to evaluate the demand-capacity ratios of structural members before proceeding with nonlinear analysis of the structures.

Table 2: Gravity and Lateral Load Consideration

Load Pattern	Loads (kN/m²)	Seismic Parameter	Load Combination
Self Wt. (DL)	As per frame wt.	S_1= 0.2, S_S= 0.50 Soil Class: SC SDC*: C, I=1, R=5.5, C_d =4.5, w_d =2.5	1) 1.4DL 2)1.2DL+1.6LF+ 0.5LR 3)1.2DL +1.6 LR+ LF 4)1.2DL + 1.0 LF + 0.5 LR+1.0E* 5) 0.9DL + 1.0E* *E -Earthquake load *SDC- Structural design category
Floor Finish (DL)	1.2		
Floor Live (LF)	3.0		
Roof Live (LR)	1.4		
Wall Load (DL)	2.4		

The capacity of the structural members remained within the allowable limit. The material's non-linear behavior is shown in Figure 4. The kinematic hardening model was considered to capture the hysteretic responses of the reinforcing bars.

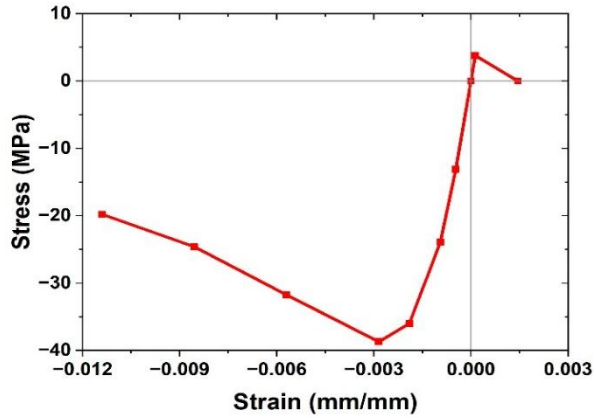

a) Concrete

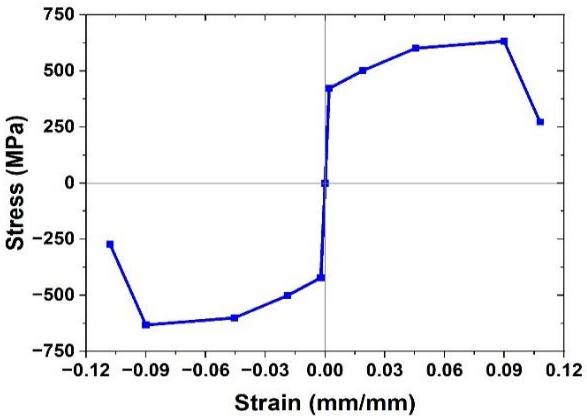

b) Rebar

Figure 4: Material nonlinearity

2.3.2 Hinge Properties

Beam and column elements were modeled as nonlinear frame elements with lumped plasticity, defining plastic hinges at both ends. User-defined deformation-controlled (ductile) plastic hinge properties were applied, with plastic hinges assumed at the element ends. Seismic performance was evaluated in accordance with FEMA 356 guidelines. Fiber hinges were used as per the ASCE standard, as shown in Figure 5. To ensure ductile flexural behavior, shear demand was kept within the capacity. Figure 5(a) presents fiber hinges: yellow for steel fiber and red for concrete fiber. Figure 5(b)- 5 (d) presents the strain limit at different performance objectives and the backbone curve of the nonlinear hinge behavior.

a) Shear wall (fiber segments): yellow color-steel; red color- concrete;

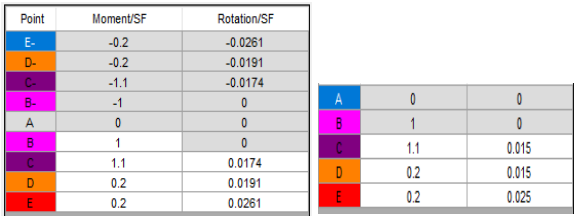

Point	Moment/SF	Rotation/SF
E-	-0.2	-0.0261
D-	-0.2	-0.0191
C-	-1.1	-0.0174
B-	-1	0
A	0	0
B	1	0
C	1.1	0.0174
D	0.2	0.0191
E	0.2	0.0261

A	0	0
B	1	0
C	1.1	0.015
D	0.2	0.015
E	0.2	0.025

b) Strain limit at a different point

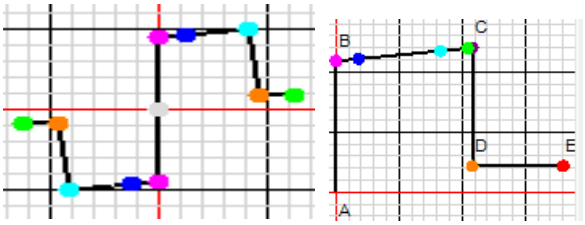

c) Backbone curve

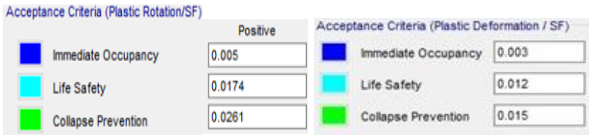

Acceptance Criteria (Plastic Rotation/SF)	Positive
Immediate Occupancy	0.005
Life Safety	0.0174
Collapse Prevention	0.0261

Acceptance Criteria (Plastic Deformation / SF)	
Immediate Occupancy	0.003
Life Safety	0.012
Collapse Prevention	0.015

d) IO, LS, and CP strain levels

Figure 5: Hinge properties of shear wall, beam, and column

2.3.3 Ground Motions

Nine pairs of ground motions (both X and Y directions) were considered in this study, as presented in Table 3. These recorded earthquakes will be scaled to approximately 0.2g to simulate a design-based earthquake (DBE). For nonlinear analysis, the FNA usually employs Ritz vectors, customized to account for P-delta effects based on gravity loads. The inclusion of

P-delta is critical for accurately determining the stability behavior.

Table 3: Reference ground motions data used in analysis

Serial	EQ Name	Year	Magnitude	PGA(g)	Scale Factor
1	ChiChi	1999	7.6	0.098	2.041
2	Holistr	1961	5.6	0.036	5.632
3	Imperia	1979	6.5	0.160	1.248
4	Kobe	1995	6.9	0.138	1.445
5	Landers	1992	7.3	0.080	2.501
6	Loma PR	1989	6.9	0.038	5.333
7	Northridge	1994	6.69	0.046	4.303
8	Trinidi	1983	5.7	0.028	7.210
9	Bhuj	2001	7.7	1.038	0.193

Nonlinear dynamic analysis uses the time history of input force or acceleration to obtain the response. These motions are applied to the 3D finite-element model developed in ETABS v16. Ground motions are matched with local seismic data, specifically the response spectrum, to represent the actual seismic demand. The time functions were scaled using SeismoMatch software to align with the target response spectra. The original time functions were adjusted to match the target acceleration values for the earthquake event. The time vs. acceleration plots for the matched and scaled response spectra are shown in Figure 6.

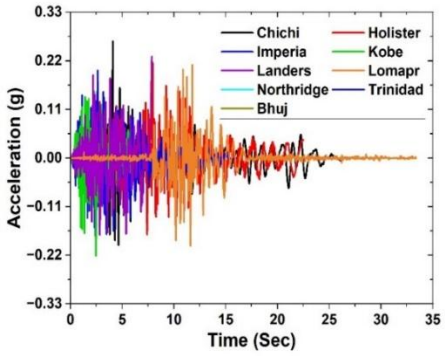

a) Matched ground motions

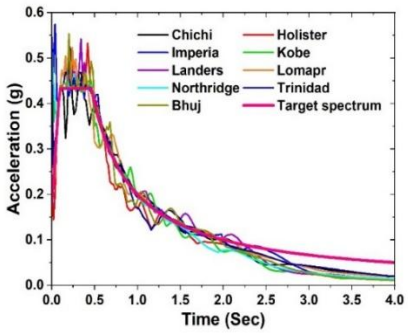

b) Scaled response spectrum

Figure 6: Matching and scaling time history ground motions

3. RESULTS AND DISCUSSIONS

3.1 Interpretation of Result for Linear Static Analysis

Based on the above considerations, a 3D finite element analysis model has been developed using commercially available software. The geometry, material properties, and loadings are strictly followed as per BNBC (2020), as mentioned earlier. In the analysis, the crack section has been considered for beams, columns, shear walls, and slabs as per the National Building Code of Bangladesh. The force-based design (FBD) approach has been used to find out the outcomes of the linear static analysis (LSA) in terms of displacement, drift, stiffness, and column demand capacity ratio.

3.1.1 Modal analysis

The building's vibration properties were determined through modal analysis. The 1st vibration mode was translation in the X direction with periods of 4.02 and 4.19 sec, the 2nd was translation in the Y direction with periods of 3.70 and 3.86 sec, the 3rd was torsion with periods of 2.33 and 2.37 sec, and the 4th was also torsion with periods of 1.24 and 1.31 sec. Twenty-six vibrational modes were considered for the modal analysis, and more than 90% of the total mass at ground level participated. The period for the first three vibrational modes is considered the fundamental period. The period, frequency, and their shapes are shown in Table 4 and Figure 7.

Table 4: Fundamental period and frequency

Mode shape no.	Before Fire Effect			After Fire Effect		
	Period	freq.	Circular freq.	Period	freq.	Circular freq.
	sec	cyc/sec	rad/sec	sec	cyc/sec	rad/sec
1	4.02	0.25	1.56	4.19	0.24	1.50
2	3.70	0.27	1.70	3.86	0.26	1.63
3	2.33	0.43	2.70	2.37	0.42	2.66
4	1.24	0.81	5.07	1.31	0.77	4.81

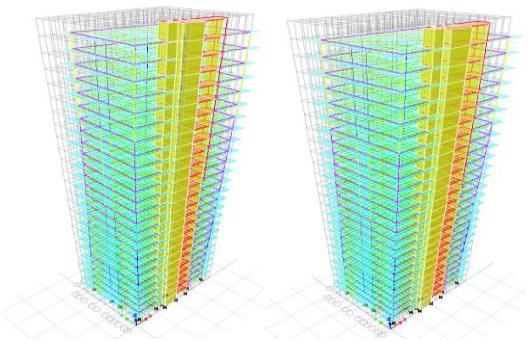

a) Mode 1 b) Mode 2

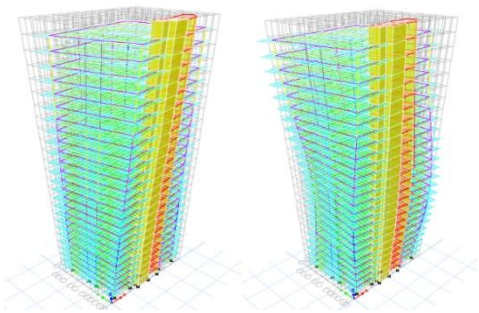

c) Mode 3 d) Mode 4

Figure 7: Deflected pattern of modal analysis

3.1.2 Moment rotation curve

A comparison of column moment-curvature between pre- and post-fire conditions for columns C1 and C2 is shown in Figure 8. The curve shows that for the same number of moments, the rotation for the post-fire condition is more than that for the pre-fire condition. Compressive strength of concrete, axial load on RC sections, and longitudinal and transverse reinforcing ratios are the parameters that affect moment-curvature relationships. Column moment capacity decreases by 11-12% for the decrease of concrete compressive strength and rebar tensile strength due to the fire effect.

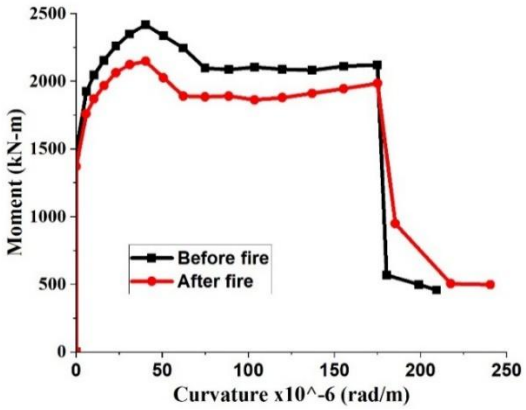

a) Column C1

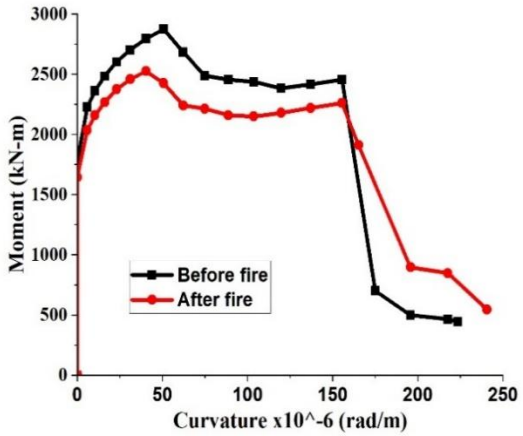

b) Column C2

Figure 8: Moment curvature curve

3.1.3 Column interaction diagram

A column interaction diagram has been prepared for pre- and post-fire conditions of C1 & C2 columns, as shown in Figure 9. Compressive strength of concrete, tensile strength, and reinforcement arrangement are parameters that affect the column interaction diagram. Column axial capacity decreases by 26 -27% at the post-fire condition compared to the pre-fire condition. Decreases may reduce the column capacity in concrete compressive strength and rebar tensile strength due to the fire effect. The weak-storey irregularity has been checked at post-fire condition following BNBC (2020) and found non-susceptible due to the fire effect.

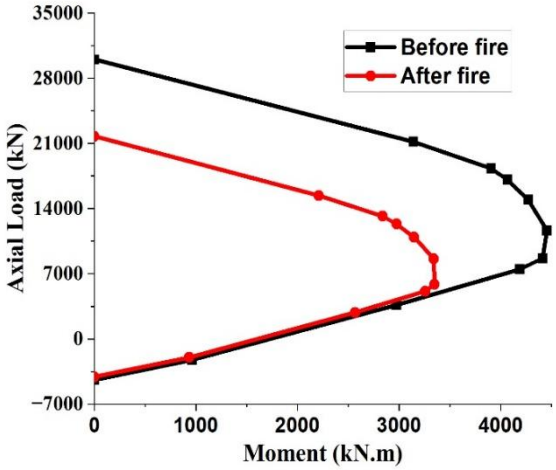

a) Column C1

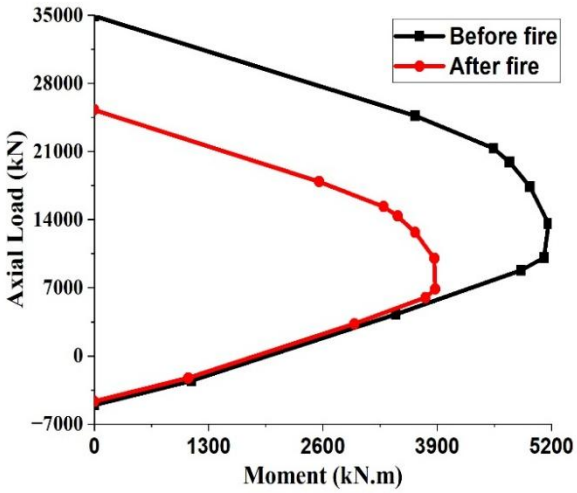

b) Column C2

Figure 9: Column Interaction Diagram

3.1.4 Deflection

The building's displacement has been determined for both axes. The increase in displacement between pre- and post-fire conditions was shown in Figure 10. Due to the fire effect, the material strength and member size have been reduced. As a result, the structure's lateral stability was reduced. The maximum displacement at the design-based earthquake is 0.961m and 1.06m at

pre- and post-fire conditions, respectively. Maximum deflection increases by about 10-20% due to a fire incident.

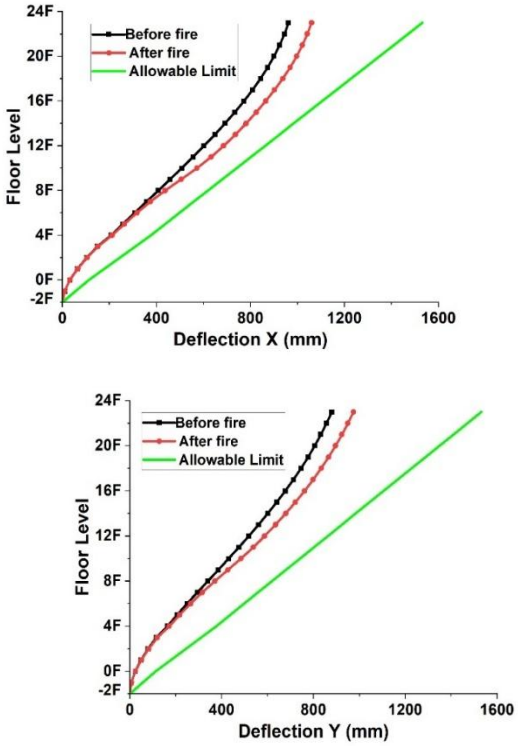

Figure 10: Story deflection

3.1.5 Story Drift

The fire effect has reduced the material capacity and the sizes of members. Due to the structural lateral capacity reduction, the drift ratio also increases by 26-37 % (Figure 11) for the fire-affected floors. The storey drift in X direction has been found beyond the allowable limit as prescribed in BNBC (2020), whereas in Y direction it has been found within the allowable limit.

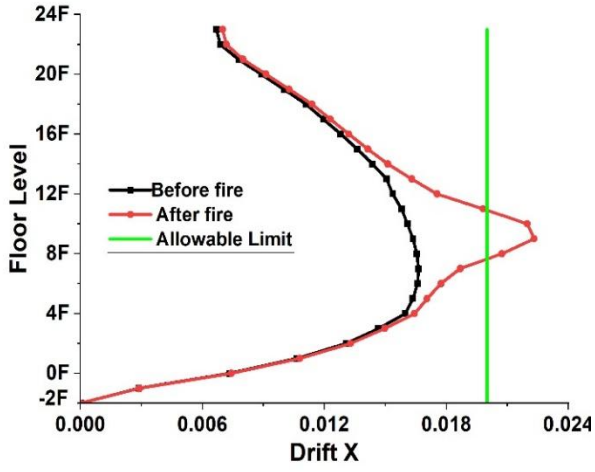

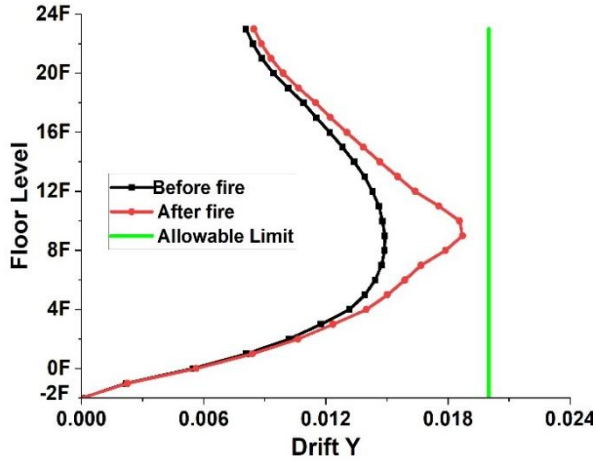

Figure 11: Story drift before and after retrofitting

3.1.6 Stiffness

The overall stiffness of the structure at different floor levels is shown in **Error! Reference source not found.**12 for both pre- and post-fire conditions. Generally, the stiffness depends on the modulus of elasticity & cross-sectional area of concrete. The stiffness of the fire-affected floor has been reduced by up to 28%. Since the strength and cross-sectional area have been reduced, stiffness is also affected. Due to reduced stiffness, the structure's displacement increases, potentially leading to soft-storey irregularity. Stiffness and deflection-based soft-storey irregularity has been checked at post-fire conditions and found to be non-existence.

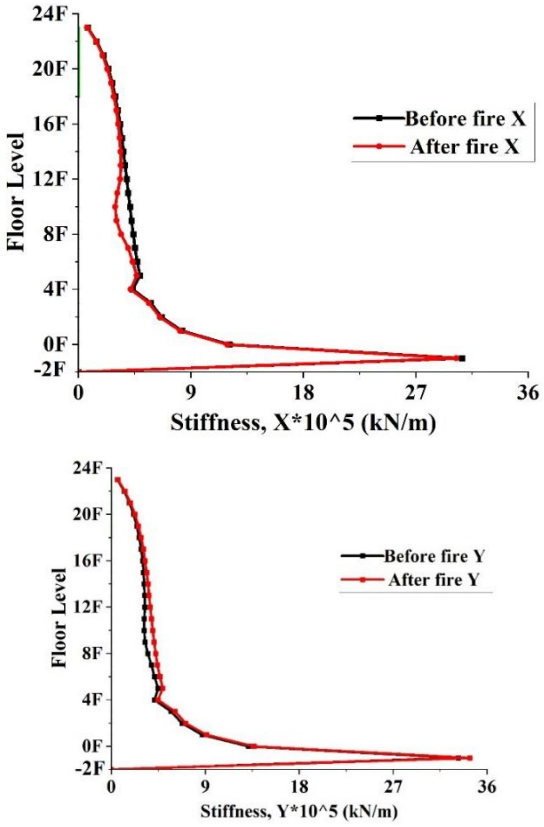

Figure 12: Stiffness of building

3.1.7 Column PMM ratio

The column demand capacity ratio is shown in Figure 13. The figure shows that the column bearing capacity is reduced. The demand capacity ratio of column C1 at grid B/10 is found within the allowable limit (<1) for pre- and post-fire conditions. However, the demand capacity ratio of the C2 column at grid B/3 is found within the allowable limit at the pre-fire condition. In contrast, the demand capacity ratio is greater than 1 for the post-fire condition. The demand capacity ratio increases by 39-43% for columns C1 and 40-42% for column C2. This may occur due to the loss of strength and stiffness of the structure.

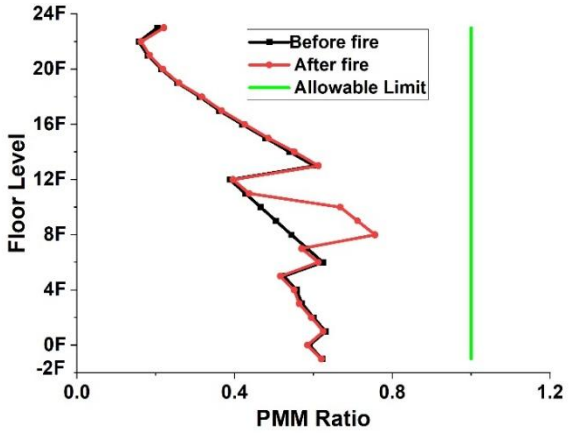

a) Column C1 at grid B-10

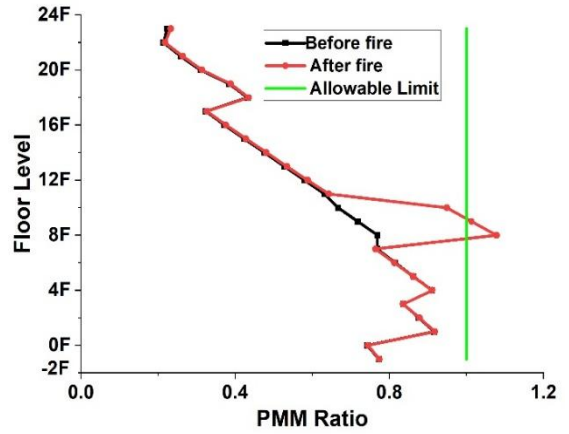

b) Column C2 at grid E-07

Figure 13: Column PMM ratio

3.1.8 Capacity of shear wall

The shear wall contributes a maximum of 47% and 55% of total base shear in X and Y directions, respectively. The shear wall's demand capacity ratio is shown in Figure 14. The figures show that the demand capacity ratios of the shear wall for post-fire conditions on the 7th, 8th, and 9th floor increases remarkably compared to pre-fire conditions. This may occur due to the structure's loss of stiffness and strength for concrete and rebar. The demand capacity ratio of shear walls W1 and W2 is found within the allowable limit (<1) at pre- and post-fire conditions.

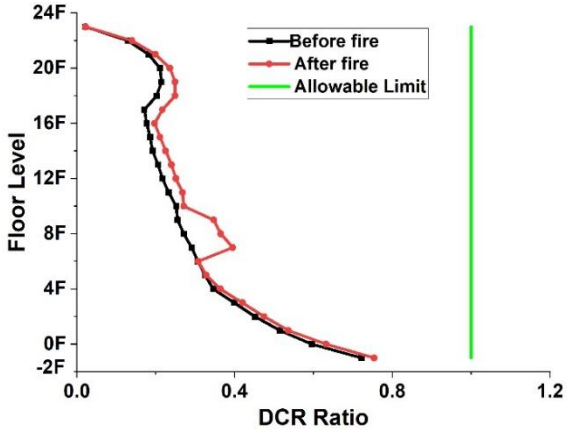

a) Shear wall W1

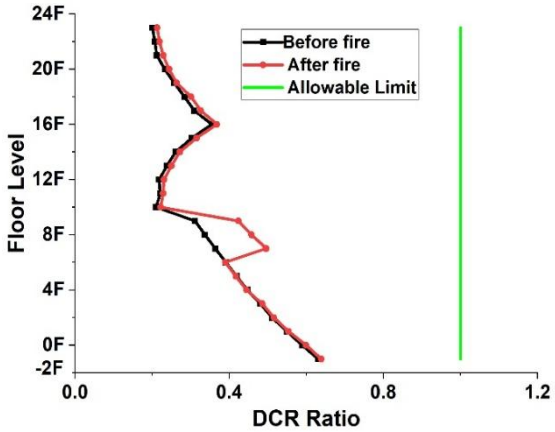

b) Shear wall W2

Figure 14: Shear wall demand-capacity ratio

3.2 Interpretation of Result for Performance-Based Analysis

Non-Linear Time History (NLTH) analysis includes ground motion with Period. Including the ground motion in NLTHA enables us to compute seismic demand. It reflects the structural displacement demand due to ground motion. Time history analysis uses the force or acceleration as input directly, which is then combined to get the response. Based on the performance-based design (PBD) by incorporating NLTHA, the following observations are made:

3.2.1 Base shear

Base shear comparisons across analyses were made for both pre- and post-fire conditions, using different time-history ground motion functions, as shown in Figure 15. The base shear values obtained from the nonlinear time-history analysis are based on nine pairs of ground motions. Figure 15 shows that the base shear resulting from the Trinidad & Hollister ground motions is considerably higher than that from the other ground motions. The maximum base shear values for different ground motions in pre- and post-fire conditions are 144156 kN & 145426 kN, respectively.

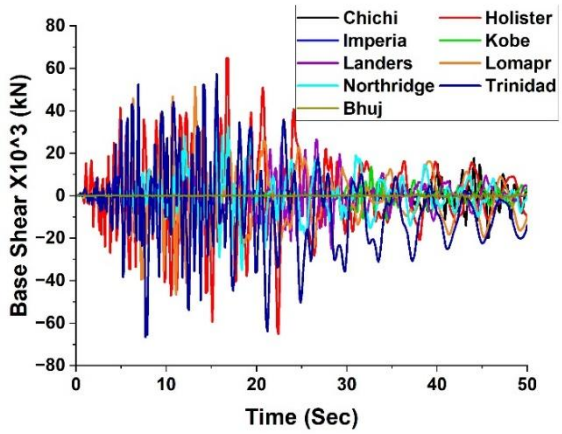

a) Before the fire condition

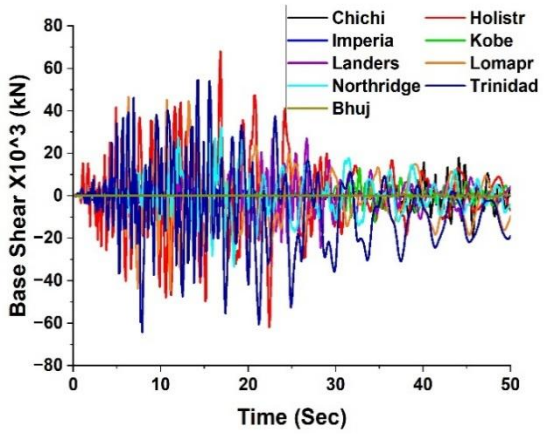

b) After fire condition

Figure 15: Base shear at different ground motions (GMs)

3.2.2 Drift ratio

The storey drift ratio of the structure for different ground motions is presented in Figure 16. The largest inter-storey drift is observed for Trinidad. Inter-storey drift ratio increased at the 7th, 8th, and 9th floors due to the fire effect. The maximum inter-storey drift ratio found is 1.1%. As per ASCE 41-13, the allowable limit states for the service and collapse prevention levels are <0.5% and <4.5%, respectively.

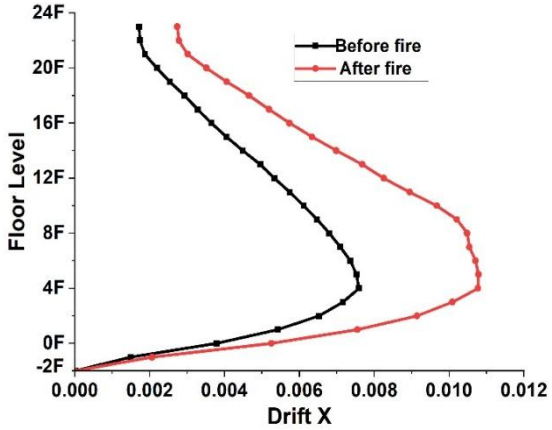

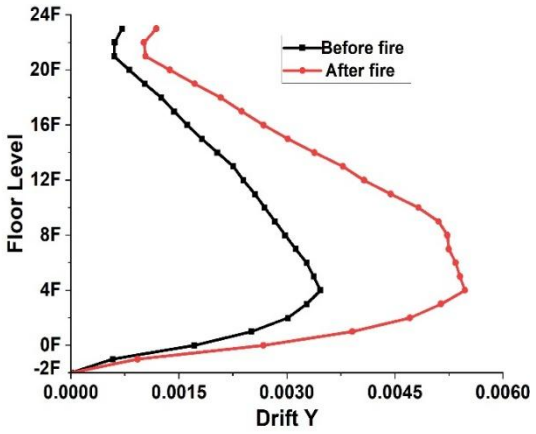

Figure 16: Maximum story drift ratio for Trinidad GMs

3.2.3 Concrete and rebar stress-strain curve

In the performance-based design philosophy, concrete and rebar strains are among the key parameters for determining the structure's internal stress-strain behavior. The stress-strain curves of rebar and concrete for different ground motions are shown in Figure 17. In both cases, the Imperial ground motion shows maximum stress for the same amount of strain.

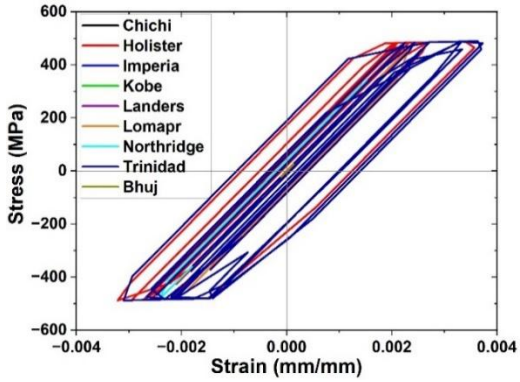

a) Rebar

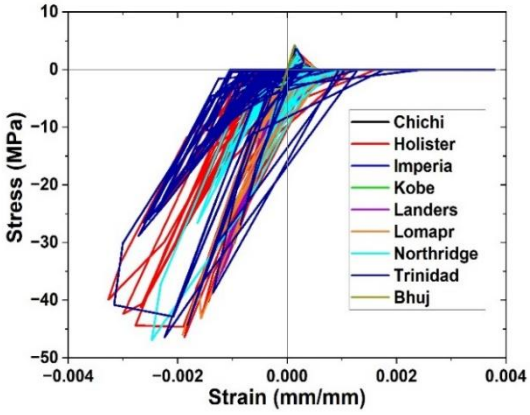

b) Concrete

Figure 17: Stress-strain curve for hinge W8H19 (8F), fiber-17

Comparative stress-strain curves for the fiber of the shear wall at the 7th, 8th, and 9th floors are presented in Figure 18 & Figure 19, respectively. Moreover, the comparative rotation and stain of the 7th-floor wall hinge have been illustrated in Figure 20. Furthermore, the fiber hinge status is also shown in Table 5. For fiber hinge states of the shear wall, all hinges are in the A-IO range. The maximum fiber strain of shear wall rebar is 0.0042 and 0.0076 for pre- and post-fire conditions, whereas the concrete strain for pre- and post-fire conditions is 0.004005 and 0.004019. According to ASCE 41-13, the allowable strain values for steel and concrete are 0.005 and 0.03, respectively.

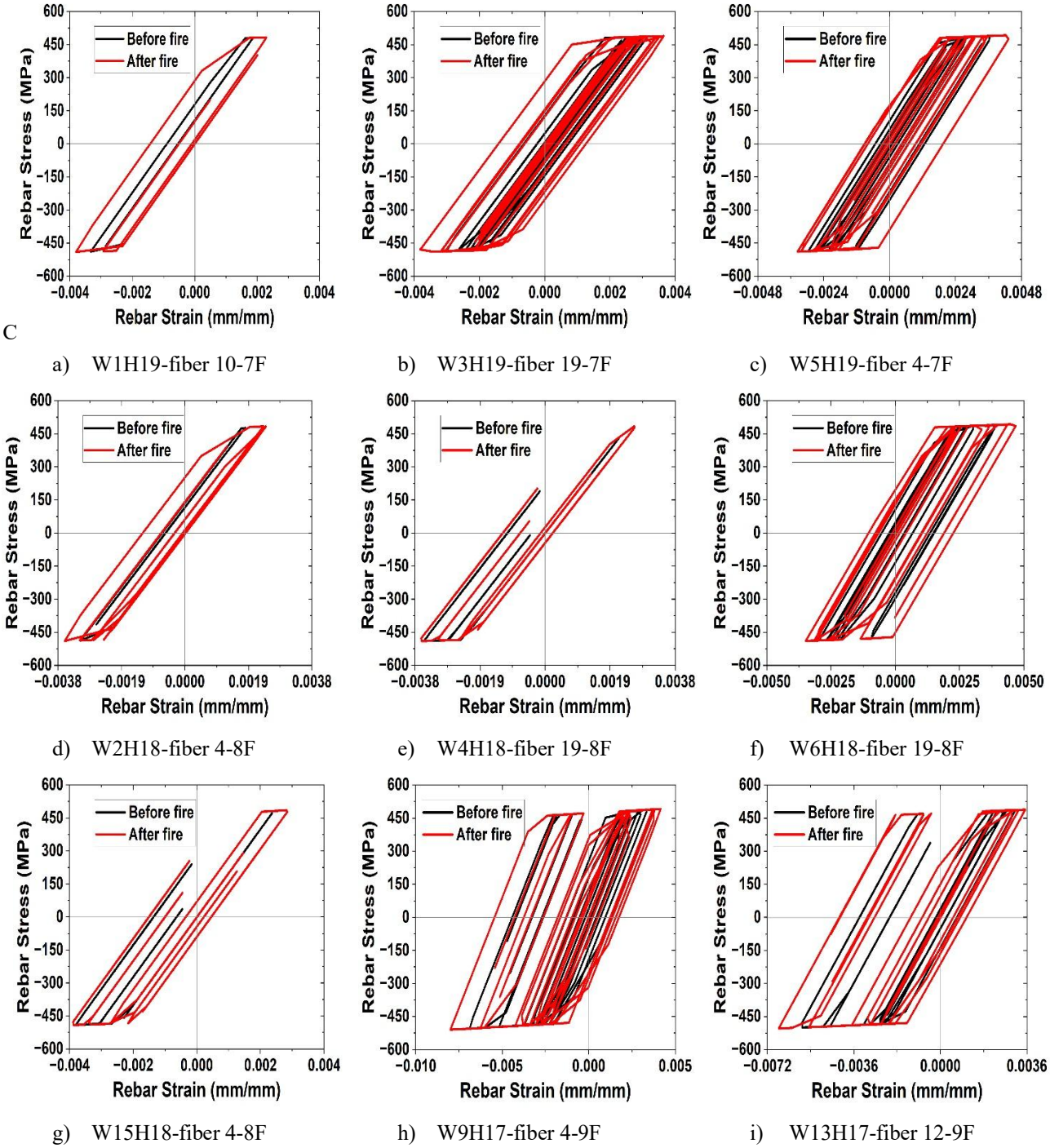

C

a) W1H19-fiber 10-7F b) W3H19-fiber 19-7F c) W5H19-fiber 4-7F

d) W2H18-fiber 4-8F e) W4H18-fiber 19-8F f) W6H18-fiber 19-8F

g) W15H18-fiber 4-8F h) W9H17-fiber 4-9F i) W13H17-fiber 12-9F

Figure 18: Fiber stress-strain curve for shear wall rebar.

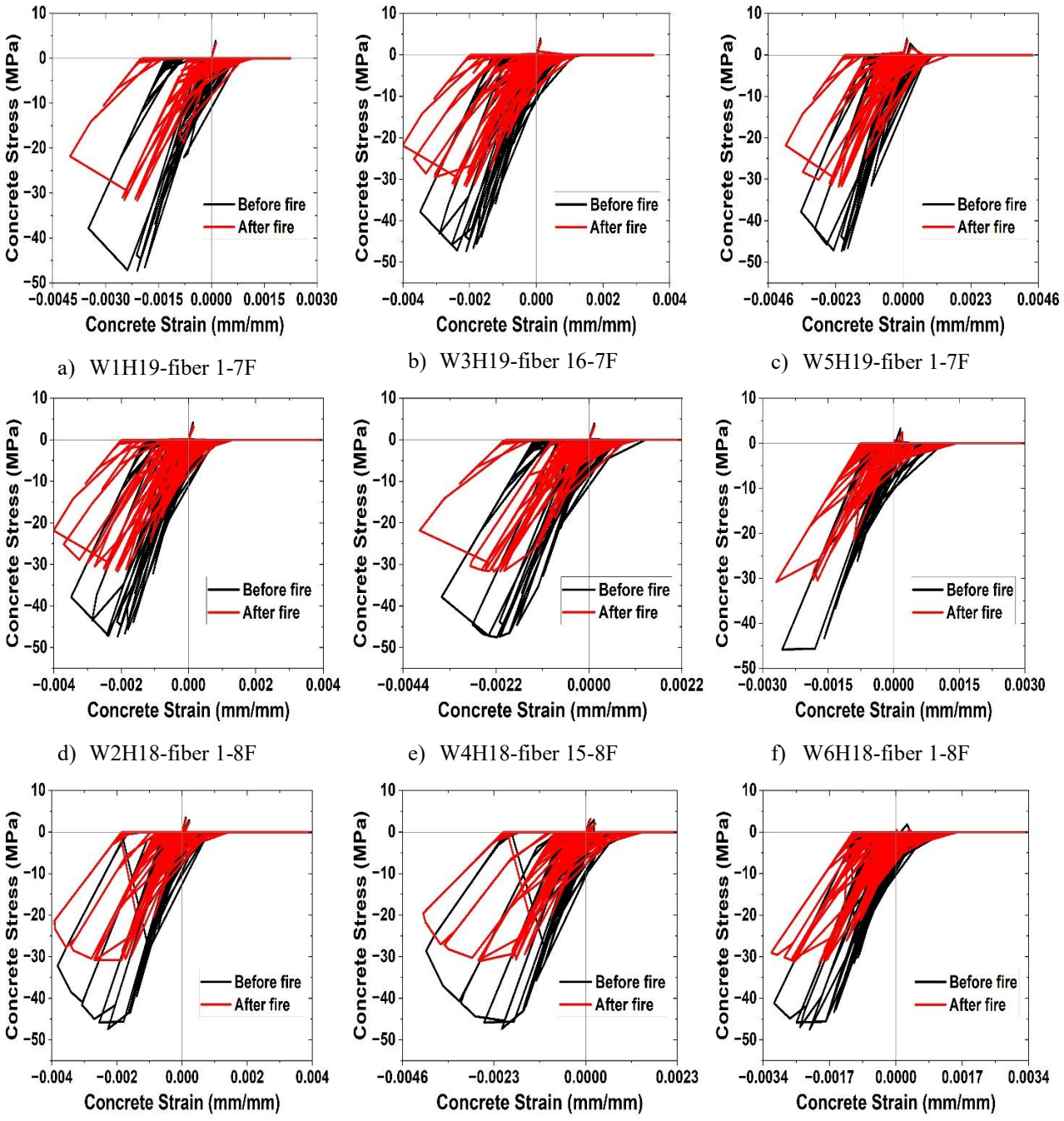

a) W1H19-fiber 1-7F b) W3H19-fiber 16-7F c) W5H19-fiber 1-7F

d) W2H18-fiber 1-8F e) W4H18-fiber 15-8F f) W6H18-fiber 1-8F

g) W15H18-fiber 1-8F h) W9H17-fiber 16-9F i) W13H17-fiber 10-9F

Figure 19: Fiber stress-strain curve for shear wall concrete.

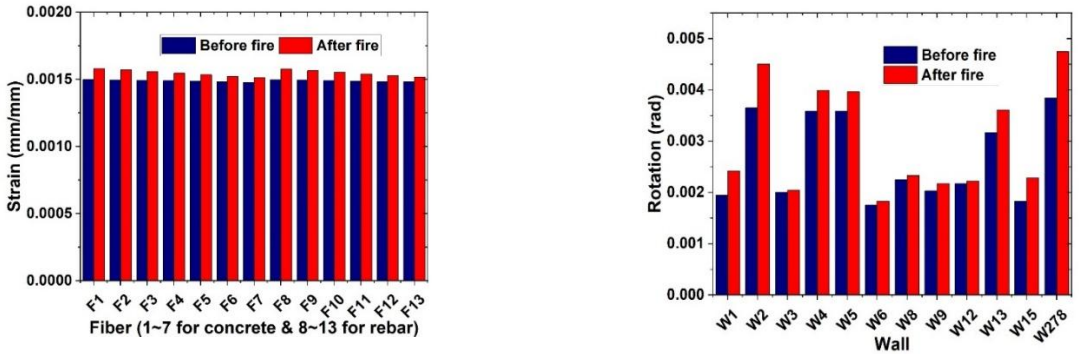

a) Fiber strain b) Wall rotation

Figure 20: Comparative strain and rotation for 7th-floor fiber hinge

Table 5: Fiber state and status of hinge-W8H19 (7F)

Fiber No.	Fiber Area	Before Fire			After Fire			Fiber Strain Increase (%)
		Fiber Stress	Fiber Strain	Fiber Status	Fiber Stress	Fiber Strain	Fiber Status	
1	112	2.66	0.00150	A to IO	2.31	0.00158	A to IO	5.4
2	224	2.56	0.00150	A to IO	2.27	0.00157	A to IO	5.0
3	224	2.42	0.00149	A to IO	2.21	0.00156	A to IO	4.4
4	224	2.28	0.00149	A to IO	2.16	0.00155	A to IO	3.9
5	224	2.13	0.00149	A to IO	2.1	0.00154	A to IO	3.3
6	224	2.01	0.00148	A to IO	2.05	0.00152	A to IO	2.8
7	112	2.06	0.00148	A to IO	2.03	0.00151	A to IO	2.4
8	8.4	299.5	0.00150	A to IO	315.2	0.00158	A to IO	5.3
9	8.4	298.8	0.00150	A to IO	312.8	0.00157	A to IO	4.7
10	8.4	298.1	0.00149	A to IO	310.4	0.00155	A to IO	4.2
11	8.4	297.3	0.00149	A to IO	308.0	0.00154	A to IO	3.6
12	8.4	296.6	0.00148	A to IO	305.6	0.00153	A to IO	3.0
13	8.4	295.9	0.00148	A to IO	303.3	0.00152	A to IO	2.5

3.2.4 Moment rotation curve

Hysteretic responses for the rotation of column and beam hinges are presented in Figure 21. Moreover, the fiber hinge status is also shown in Table 6. Hysteretic responses of the wall hinge at the 7th, 8th, and 9th floor levels are presented in Figure 22. The colours of different ground motions clearly highlight their hysteretic moment-rotation responses. The maximum hinge rotation of the shear wall for pre- and post-fire conditions is 0.009 rad and 0.0011 rad, respectively. The amount of moment-carrying capacity of the wall also depends on the size and direction of the wall with respect to the ground motions.

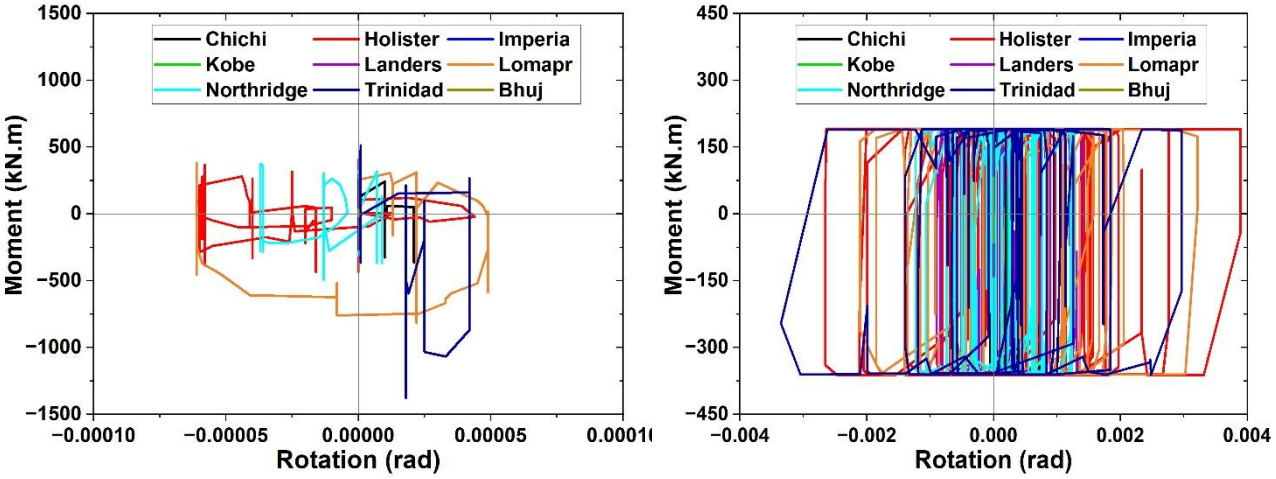

a) Column Hinge C2H31(8F) b) Beam hinge B2H29(8F)

Figure 21: Hysteretic response of hinge for different GMs

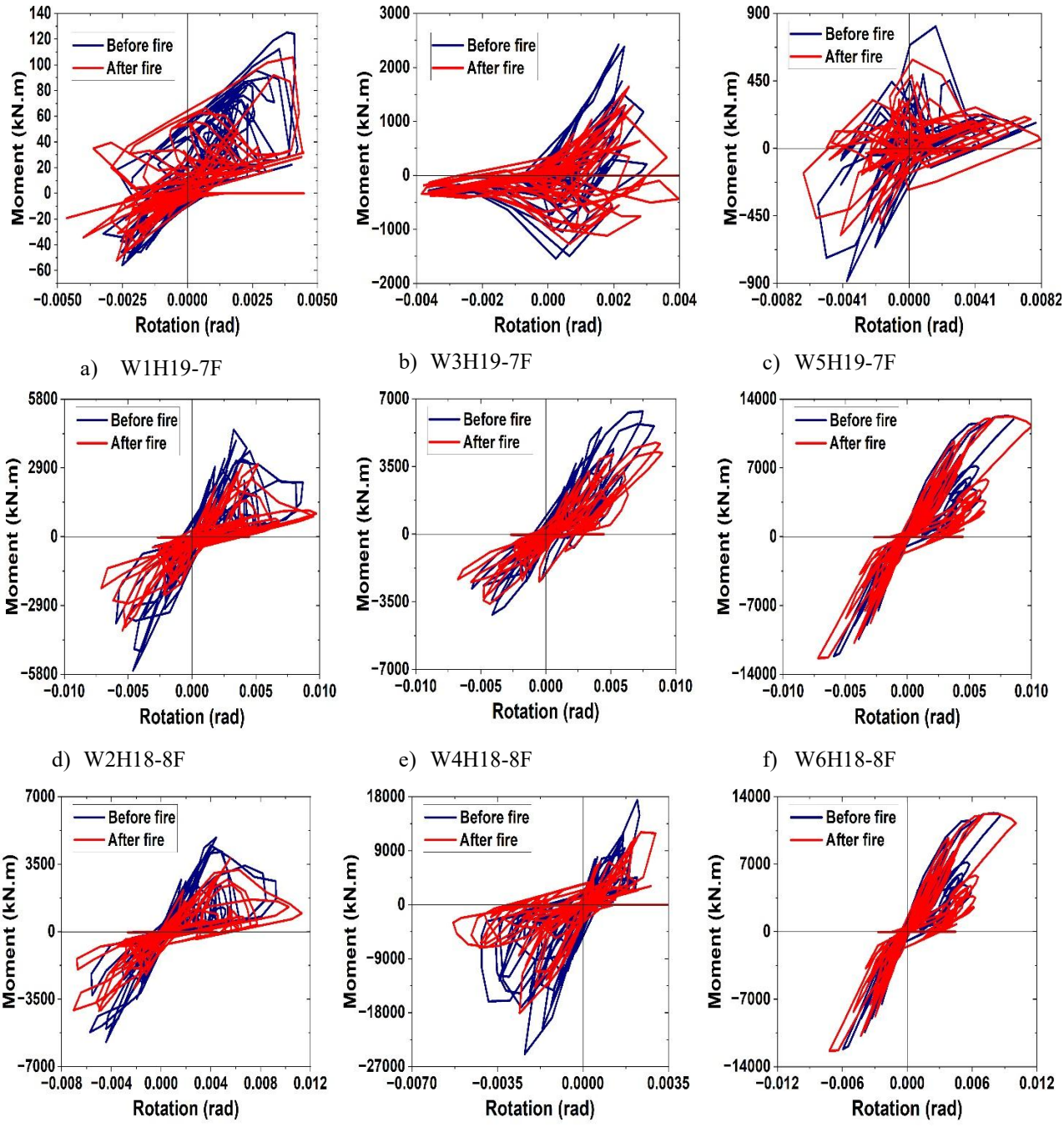

a) W1H19-7F b) W3H19-7F c) W5H19-7F

d) W2H18-8F e) W4H18-8F f) W6H18-8F

g) W2H17-9F h) W6H17-9F i) W278H16-9F

Figure 22: Hinge moment rotation curve for shear wall.

Table 6: Hinge state and status of 7th-floor wall

Wall	Fiber No.	Fiber Area	Before Fire			After Fire			Fiber Rotation Increase (%)
			Moment (kN-m)	Rotation (rad)	Fiber Status	Moment (kN-m)	Rotation (rad)	Fiber Status	
W1	1	112	43	0.0019	A to IO	49	0.0024	A to IO	24.6
W2	2	224	4645	0.0036	A to IO	3572	0.0045	A to IO	23.5
W3	3	224	2239	0.0020	A to IO	1526	0.0020	A to IO	1.9
W4	4	224	5016	0.0036	A to IO	3793	0.0040	A to IO	11.3
W5	5	224	289	0.0036	A to IO	279	0.0040	A to IO	10.6
W6	6	224	13643	0.0018	A to IO	8192	0.0018	A to IO	4.1
W8	7	112	48	0.0023	A to IO	41	0.0023	A to IO	3.3

W9	8	8.4	105	0.0020	A to IO	115	0.0022	A to IO	7.1
W12	9	8.4	109	0.0022	A to IO	107	0.0022	A to IO	2.3
W13	10	8.4	10973	0.0032	A to IO	8203	0.0036	A to IO	14.1
W15	11	8.4	159	0.0018	A to IO	118	0.0023	A to IO	24.8
W278	12	8.4	10169	0.0038	A to IO	9105	0.0047	A to IO	23.5

4. CONCLUSIONS

In this study, an assessment of a fire-damaged RC commercial building was conducted using linear static and nonlinear dynamic analyses. The 7th, 8th, and 9th floor of the building was damaged during the fire. Due to the duration and the elevated temperatures during the fire, some structural elements were severely damaged. The following conclusions were drawn from the study:

- The decrease in the cross-sectional area of the beams and column capitals due to spalling and removal of the concrete cover reduced the bond between the longitudinal reinforcement and concrete. Considering the bond loss between concrete and reinforcement due to decreased material strength, the load-carrying capacities of the column, beams, and slabs decreased.
- A few columns were found to be overloaded. This may be due to the loss of concrete strength and rebar from fire damage.
- Moreover, hinge rotation of beam, column, and shear wall at pre-fire condition is found to be greater than the post-fire condition.
- The building shows greater deflection and drift ratio at the post-fire condition than at the pre-fire condition. This may have occurred due to a loss of stability at high temperatures.

In conclusion, localized damage was observed in the fire-damaged building. The columns, beams, and shear walls are not damaged significantly.

ACKNOWLEDGEMENT

The authors are pleased to acknowledge the technical support provided by the Center for Advisory & Testing Services of Civil Engineering Department (CATS-CE) and the financial support of MIST, Dhaka, Bangladesh. The authors would also like to acknowledge the contributions of the lab technicians from the concrete and SM labs of the Civil Engineering Department of MIST.

DATA AVAILABILITY STATEMENT

Datasets generated during the current study are available from the corresponding author upon reasonable request.

FUNDING DECLARATION

This research was self-funded.

ETHICS APPROVAL

This study is an engineering experimental investigation. The MIJST Research Ethics Committee has confirmed that formal ethical approval was not required.

ETHICS, CONSENT TO PARTICIPATE, AND CONSENT TO PUBLISH

Not applicable.

COMPETING INTERESTS

The authors declare that they have no competing interests.

AUTHOR CONTRIBUTIONS

Author 1: Writing – Original draft, Visualisation, Validation, Software, Investigation.

Author 2: Writing – Review & editing, Validation, Investigation, Conceptualisation..

ARTIFICIAL INTELLIGENCE ASSISTANCE STATEMENT

Portions of this manuscript were assisted by an artificial intelligence language model (ChatGPT, OpenAI). The tool was used solely for language editing, text refinement, and improving clarity. All content, data interpretation, analysis, conclusions, and final decisions were produced, verified, and approved by the authors. The authors take full responsibility for the accuracy and integrity of the manuscript.

CONFLICT OF INTEREST DECLARATION

The authors declare that they have no conflicts of interest.

REFERENCES

Ali, F., O'Connor, D., & Abu-Tair, A. I. (2001). Explosive spalling of high-strength concrete columns in fire. *Magazine of Concrete Research*, 53(3), 197–204. https://doi.org/10.1680/macr.2001.53.3.197

Anam, I., Shoma, Z., & Talukder, A. (2003). Nonlinear seismic response of Reinforced Concrete structures. In *Conference on Advances in Structures: Steel, Concrete, Composite & Aluminum-2003* (pp. 475–481). Sydney, Australia.

Anderberg, Y., & Thelandersson, S. (1976). Stress and deformation characteristics of concrete at high temperatures: Experimental investigation and material behaviour model (Bulletin 54). Lund Institute of Technology.

Bailey, C. G. (2002). Holistic behaviour of concrete buildings in fire. *Proceedings of the Institution of Civil Engineers - Structures and Buildings*, 152(3), 199–212. https://doi.org/10.1680/stbu.2002.152.3.199

Bailey, C. G. (2004). Structural fire design: Core or specialist subject? *The Structural Engineer*, 82(9), 32–38.

Benýšek, M., Štefan, R., & Procházka, J. (2020). Effect of fire model parameter variability on determination of fire resistance of concrete structural members. *Solid State Phenomena*, 309, 165–172. https://doi.org/10.4028/www.scientific.net/SSP.309.165

Block, F., Yu, C., & Butterworth, N. (2010). The practical application of structural fire engineering on a retail development in the UK. *Journal of Structural Fire Engineering*, 1(4), 205–218. https://doi.org/10.1260/2040-2317.1.4.205

Chan, S. Y. N., Luo, X., & Sun, W. (2000). Effect of high temperature and cooling regimes on the compressive strength and pore properties of high-performance concrete. *Construction and Building Materials*, 14(5), 261–266. https://doi.org/10.1016/S0950-0618(00)00031-3

Duan, H., & Hueste, M. B. D. (2012). Seismic performance of a reinforced concrete frame building in China. *Engineering Structures*, 41, 77–89. https://doi.org/10.1016/j.engstruct.2012.03.030

BSI. (2002). Eurocode 1: Actions on structures — Part 1-2: General actions — Actions on structures exposed to fire (BS EN 1991-1-2:2002). British Standards Institution.

Felicetti, R. (2013). Assessment methods of fire damages in concrete tunnel linings. *Fire Technology*, 49(2), 509–529. https://doi.org/10.1007/s10694-012-0272-8

Felicetti, R. (2014). Assessment of fire damage in concrete structures: New inspection tools and combined interpretation of results. In *Proceedings of the 8th International Conference on Structures in Fire (SiF'14)* (pp. 513–520). Shanghai, China.

Galal, K. E., & Ghobarah, A. (2003). Flexural and shear hysteretic behaviour of reinforced concrete columns with variable axial load. *Engineering Structures,* 25(11), 1353–1367. https://doi.org/10.1016/S0141-0296(03)00111-1

Huang, Z. (2010). The behaviour of reinforced concrete slabs in fire. *Fire Safety Journal*, 45(5), 271–282. https://doi.org/10.1016/j.firesaf.2010.05.001

Jiang, F., Zhu, C., & Xue, J. (2007). Nonlinear analysis of load-carrying capacity for bar buckling based on arc-length method. *Building Science*, 23(11), 9–12.

Jowsey, A., Torero, J. L., Usmani, A., Lane, B., & Lamont, S. (2005). Determination of fire induced collapse mechanisms of multi-storey steel framed structures - A case study. In *Proceedings of the 10th International Fire Science and Engineering Conference* (Interflam, 2004) (pp. 1293–1304). Interscience Communications.

Keerthan, P., & Mahendran, M. (2013). Thermal performance of composite panels under fire conditions using numerical studies: Plasterboards, rockwool, glass fibre, and cellulose insulations. Fire Technology, 49(2), 329–356. https://doi.org/10.1007/s10694-012-0266-6

Khoury, G. A. (2000). Effect of fire on concrete and concrete structures. Progress in Structural Engineering and Materials, 2(4), 429–447. https://doi.org/10.1002/pse.51

Kordina, K., & Krampf, L. (1984). Empfehlungen für brandschutztechnisch richtiges Konstruieren von Betonbauwerken [Recommendations for fire-safe construction of concrete structures]. Deutscher Ausschuss für Stahlbeton, 352, 7–34.

Lie, T. T., Allen, D. E., & Lin, T. D. (1972). Calculation of the fire resistance of reinforced concrete columns (Technical Paper No. 378). National Research Council of Canada, Division of Building Research.

Lin, W.-M., Lin, T. D., & Powers-Couche, L. (1996). Microstructures of fire-damaged concrete. *ACI Materials Journal*, 93(3), 199–205. https://doi.org/10.14359/9809

Lu, Y. (2002). Comparative study of seismic behavior of multistory reinforced concrete framed structures. *Journal of Structural Engineering*, 128(2), 169–178. https://doi.org/10.1061/(ASCE)0733-9445(2002)128:2(169)

Ma, Z., & Mäkeläinen, P. (2000). Parametric temperature–time curves of medium compartment fires for structural design. *Fire Safety Journal*, 34(4), 361–375. https://doi.org/10.1016/S0379-7112(00)00009-4

Mallick, D., Momin, M. A., Arpan, D., & Rahman, N. U. (2026). Performance assessment of masonry infilled RC frame by pushover analysis. In *Proceedings of the 8th International Conference on Civil Engineering for Sustainable Development (ICCESD 2026)*. KUET, Khulna, Bangladesh.

Mo, Y. L., Hwang, C. H., & Wang, J. S. (2004). Seismic response of fire-damaged reinforced concrete buildings. *Advances in Structural Engineering*, 7(1), 95–109. https://doi.org/10.1260/136943304322984796

Momin, M. A., Ahmed, K. S., Mustafy, T., & Islam, M. J. (2024). Damage assessment and test results of construction materials of a fire-damaged RC building. *Results in Engineering*, 24, Article

102986. https://doi.org/10.1016/j.rineng.2024.102986

Neves, I. C., Rodrigues, J. P. C., & Loureiro, A. d. P. (1996). Mechanical properties of reinforcing and prestressing steels after heating. *Journal of Materials in Civil Engineering*, 8(4), 189–194. https://doi.org/10.1061/(ASCE)0899-1561(1996)8:4(189)

Poliakova, T., & Grigoryan, M. (2018). Fire safety issues in the design and construction of high-rise buildings. MATEC Web of Conferences, 251, Article 05018. https://doi.org/10.1051/matecconf/201825105018

Roufaiel, M. S., & Meyer, C. (1987). Analytical modeling of hysteretic behavior of R/C frames. *Journal of Structural Engineering*, 113(3), 429–444. https://doi.org/10.1061/(ASCE)0733-9445(1987)113:3(429)

Sadjadi, R., Kianoush, M. R., & Talebi, S. (2007). Seismic performance of reinforced concrete moment resisting frames. *Engineering Structures*, 29(9), 2365–2380. https://doi.org/10.1016/j.engstruct.2006.11.029

Sengupta, P., & Li, B. (2014). Hysteresis behavior of reinforced concrete walls.*Journal of Structural Engineering*, 140(7), Article 04014030. https://doi.org/10.1061/(ASCE)ST.1943-541X.0000951

Seo, J., Hu, J. W., & Davaajamts, B. (2015). Seismic performance evaluation of multistory reinforced concrete moment resisting frame structure with shear walls. Sustainability, 7(10), 14287–14308. https://doi.org/10.3390/su71014287

Tovey, A. K. (1986). Assessment and repair of fire-damaged concrete structures—an update. *Special Publication*, 92, 47–62. https://doi.org/10.14359/2464

Wang, Y., Marsden, J., & Kelly, M. (2011). Challenges of fire fighting in fire engineered built environment. *Procedia Engineering*, 11, 583–592. https://doi.org/10.1016/j.proeng.2011.04.699

Xun-Liu, W., Xin-Zheng, L., & Lie-Ping, Y. (2007). Numerical simulation for the hysteresis behavior of RC columns under cyclic loads. Engineering Mechanics, 24(12), 76–81.

Zehfuss, J., & Hosser, D. (2007). A parametric natural fire model for the structural fire design of multi-storey buildings. *Fire Safety Journal*, 42(2), 115–126. https://doi.org/10.1016/j.firesaf.2006.08.004